S. Varaksin[1], B. Hamidi[2], J. Racinais[3]

Chairman
[1] Chairman, ISSMGE TC211, [2] Curtin University, [3] Menard

The Thin Line between Deep Foundations and Soil Improvement

Abstract

Deep foundations have been the historical and conventional solution to support heavy loads in poor capacity_soils; however during the past decades ground improvement has successfully been able to provide competitive and economical technical foundation solutions by increasing the ground mechanical properties, and thereby increasing bearing capacity, and reducing total, differential, and creep settlements. More recent ground improvement techniques, such as Controlled Modulus Columns (CMC), that are based on the concept of introducing cementitious columnar inclusions into soft grounds are often confused with in-situ piling methods. This paper will discuss the concept of CMC, its design philosophy, the way it behaves and a case study will be presented to demonstrate its application.

Keywords: Controlled Modulus Columns, CMC, ground improvement, rigid inclusion, arching, Eurocode, ASIRI

Introduction

Historically, deep foundations have been designed and constructed to support heavy loads in poor and unfavorable ground conditions. The main purpose of these foundations is to transfer the full load of the structure through pile caps, structural slabs, or grade beams to competent subsoil by “bridging” the compressible soft soils.

The notion of soil improvement has been subject to relatively rapid developments in the last half century. More recently, Chu et al. [1] have categorized and described the various ground improvement techniques in the State of the Art report of ISSMGE TC211 that was published at the 17th International Conference of Soil Mechanics and Geotechnical Engineering in 2009. Category C of Table 1 refers to ground improvement techniques with admixtures or inclusions. In these methods, columnar inclusions are installed in the ground, and the loads are distributed between the in-situ soft soil and inclusions through a superficial transition layer or load transfer platform (LTP) by arching [2]. Thus, as load concentration is reduced the superstructure does not have to connect to the inclusions by structural elements, and the LTP will efficiently suffice. Each technique in this category has its benefits and limitations, for example dynamic replacement is a very cost effective ground improvement technique, but is applicable to treatment of soft ground to depths of approximately 5 m, and stone columns can be installed to greater depths, but may bulge due to insufficient peripheral in-situ soil restraining [3].

One of the ground improvement techniques in Category C that was developed by Menard in 1994 [1], and is being implemented in more and more projects throughout the world is called Controlled Modulus Columns, which is frequently abbreviated to CMC. This technology is composed of rigid cementitious columnar inclusions that are not bound by very soft ground conditions that cannot provide lateral constraint. Due to the installation equipment, the appearances of the columns, which resemble unreinforced piles, and their superior ability in limiting settlements compared to other ground improvement techniques with inclusions, such as stone columns, CMC are frequently and erroneously referred to as piles, but their concept, design and behavior distinguishes them from piles.

Controlled Modulus Columns

CMC are installed in soft ground using a specially designed auger that, as shown in Fig. 1, is composed of a penetrating helical tip and a pseudo-cylindrical hollow stem follow-up section. As the auger penetrates the soil by screwing, the pseudo-cylindrical section displaces the soil laterally, and reduces the amount of spoil that is generated by this technology to negligible amounts compared to cast in-situ piling solutions such as CFA or bored piles. During the auger extraction process, grout is pumped through the hollow auger to form a columnar inclusion with a diameter that is usually 250 to 450 mm.

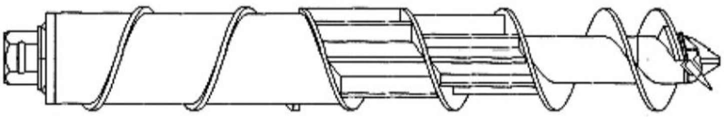

Fig. 1. CMC auger

Unlike stone columns whose stability relies on the horizontal containment of the soil or deep soil mixing where column strength is dependent on the in-situ soil properties, CMC do not rely on external parameters for lateral stability nor is their strength affected by the surrounding soil. In fact column strength can be fully controlled simply by varying the strength of the grout. Thus this method can reduce settlements more efficiently compared to other techniques in which inclusions are installed in the soil.

As the deformation modulus of CMC are typically 50 to 3,000 times that of the weakest soil stratum [4] it is possible to greatly reduce ground settlements using a lower replacement ratio (which is the ratio of an inclusion area to total unit cell area [5, 6]) when comparing with inclusions are composed of granular material.

The amount of vibration that is generated by CMC installation is comparable with CFA piling as the installation process itself is vibration free, and measured vibrations originate from the base machine. This characteristic can make CMC the preferred choice over other Category C ground improvement techniques such as dynamic replacement in which granular inclusions are dynamically driven into the ground by dropping a heavy pounder from considerable height or stone columns in which granular inclusions are formed by water jetting and vibrating a vibroflot.

The CMC rig should be able to provide a continuous down pull with a high torque in rotation. The torque is typically in the range of 20 tm, continuous pull down is in the range of 20 t, and rotation speed is in the order of 15 rpm. Further enhancements to the equipment can include a radio control unit to allow the rig operator to directly command the concrete pump from his control panel. The control panel displays torque, speed, depth, down pull force, grout pressure and volume of pumped grout. Fig. 2 shows the installation of CMCs in two projects in France.

The main advantages of CMC can thus be summarized as:

- CMC strength is independent of the in-situ soil.
- With similar replacement ratios, the magnitude of settlement reduction using CMC is much larger than in ground improvement methods that use granular material for inclusions.
- CMC does not rely on external parameters for lateral stability
- CMC installation process is vibration free, and measured vibrations solely originate from the rig.

- CMC are installed by laterally displacing the soil; hence negligible volumes of spoil is produced that makes this foundation solution attractive when work is carried out in contaminated sites or when spoil removal is expensive.
- CMC installation rate is very high.

Fig. 2. Installation of CMC columns in two projects in France

Design and Recent Advances

Combarieu [7] has studied the behavior of rigid inclusions that are installed in soft ground. As shown in Figure 3, A compressible ground of thickness H that is subjected to an embankment load with intensity q_o will ultimately settle an amount on the surface that can be denoted by $W_s(o)$. Likewise the settlement at any depth can be denoted by $W_s(z)$.

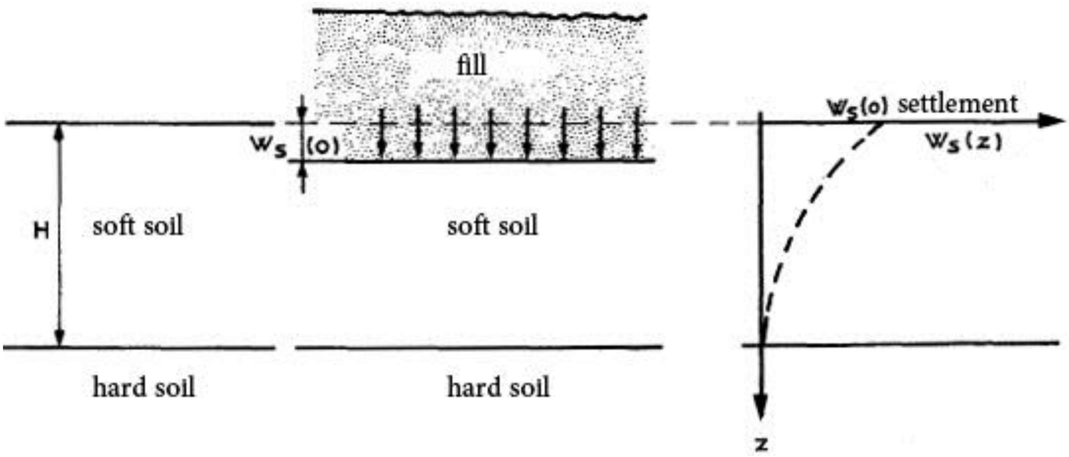

Fig. 3. Ground section without rigid inclusion [7]

Combarieu then examined the equilibrium conditions of a single rigid inclusion after complete stabilization. The soil conditions at distances away from the single inclusion are identical to untreated ground shown in Fig. 3. However, the stress and deformations change around the immediate vicinity of the inclusion. The Inclusion settles by an amount equal to $W_p(z)$ due to the loading plus a further small amount due to its own compression (since it is not infinitely rigid). Obviously, the settlement would be higher for the case shown in Fig. 4 where the rigid inclusion is resting on soft soil compared to Fig. 5 where the rigid inclusion is resting on hard soil.

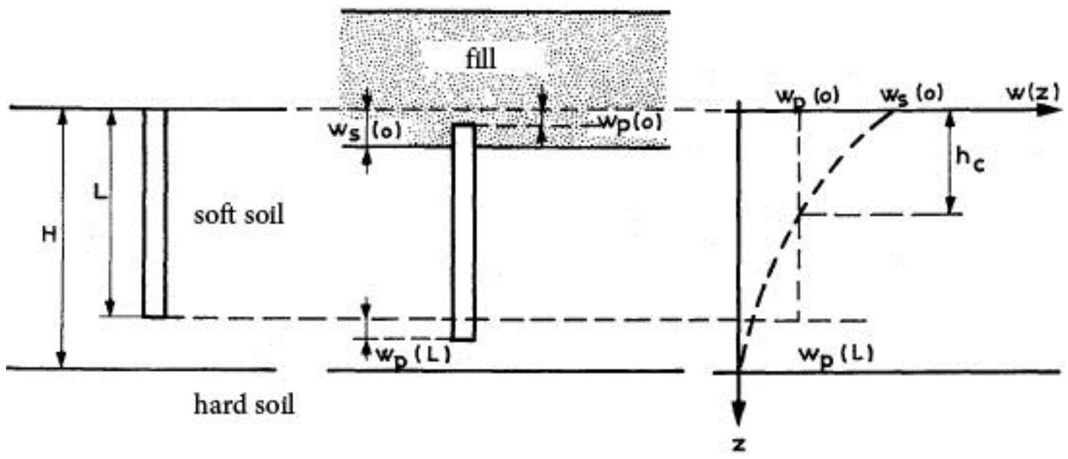

Fig. 4. Ground section with rigid inclusion in soft ground [7]

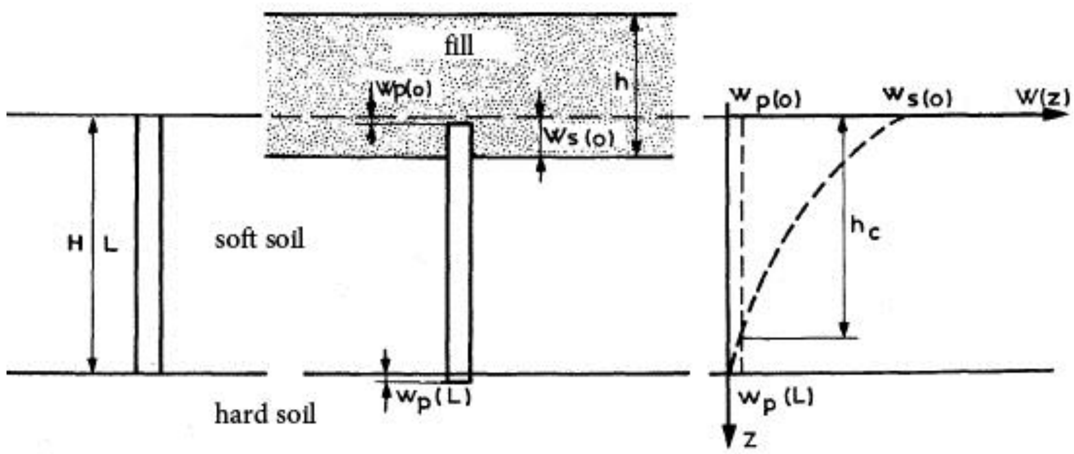

Fig. 5. Ground section with rigid inclusion in hard ground [7]

The top of the inclusion punches through the embankment by an amount that is equal to $W_s(o)$ - $W_p(o)$. At this level the head of the inclusion behaves like an anchor plate that is embedded in the thickness of the embankment, and develops traction forces from the surface.

At the lower part of the inclusion where $z>h_c$, the settlement of the soil is smaller than the inclusion settlement and inclusion compression; however the opposite is true in the upper part where $z<h_c$. Soil and inclusion settlement are equal at $z=h_c$.

Ultimately, as shown in Fig. 6, the four forces acting along the inclusion at equilibrium are:

Driving forces: The vertical load Q acts on the head of the inclusion, akin to an anchor, and the resultant negative friction, F_n, acts along the inclusion segment with length h_c.

Resisting forces: Positive friction, F_p, is mobilized in lower part of the inclusion and along a segment with length L - h_c, and Q_p acts at the base of the inclusion. The balance of the forces is $Q + F_n = F_p + Q_p$.

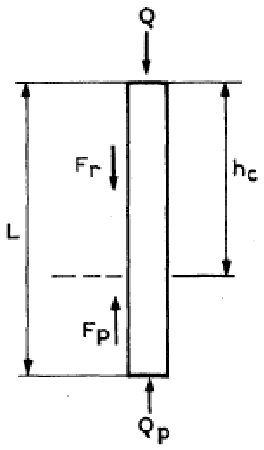

Fig. 6. Forces acting on the rigid inclusion [7]

The combined effect of a cementitious columnar inclusion with no rigid connection to the structure has been the object of a French nationwide research program called ASIRI (Améliorations de Sols par Inclusions RIgides, which translates to Soil Improvement by Rigid Inclusions) [8], in which the Bridges and Highways Administration, consultants and specialty contractors have jointly carried out a detailed investigation to understand the behavior of rigid inclusions that support slabs or embankments. Two major parts in the ASIRI are dedicated to the behavior of the load transfer platform and the determination of the limiting pressure at the top of the inclusions and the design of slab on grades supported by soil that has been reinforced with rigid inclusions. LTP behavior and limiting pressures at the top of the inclusions will be reviewed in this paper.

Behavior of the Load Transfer Platform

As shown in Fig. 7, it is assumed that rigid inclusions with diameter $D= 2r_p$ are installed in a square grid of dimension s. LTP thickness is denoted by H_M and is defined by its characteristics (cohesion c', friction angle φ' and volumetric weight γ). The uniformly distributed external load q_o is applied to the LTP.

ASIRI has shown that while the actual equilibrium diagram depends on the geometry and nature of the loading, as shown in Fig. 8, two failure mechanisms are possible. The Prandtl mechanism [9] occurs when the LTP is covered by a rigid structural element such as a slab on grade, raft or footings or when the embankment thickness is sufficient to avoid the punching failure mechanism. The punching failure mechanism corresponds to the realization of a shear cone in the LTP's surface, for example in the case of a thin road embankment. ASIRI implies that an embankment is considered thin when:

$$H_M < 0.7(s - D)$$

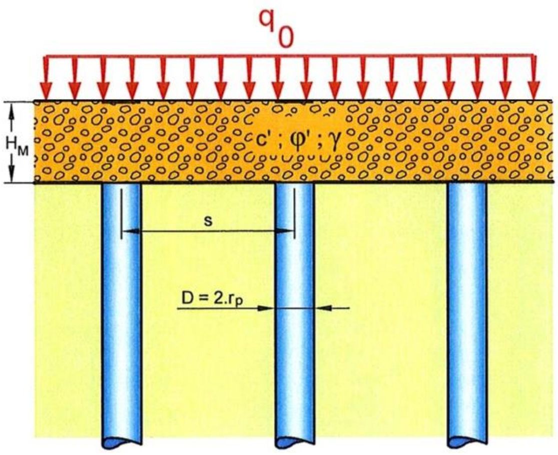

Fig. 7. Section showing ground improved by rigid inclusions, LTP and uniform loading [8]

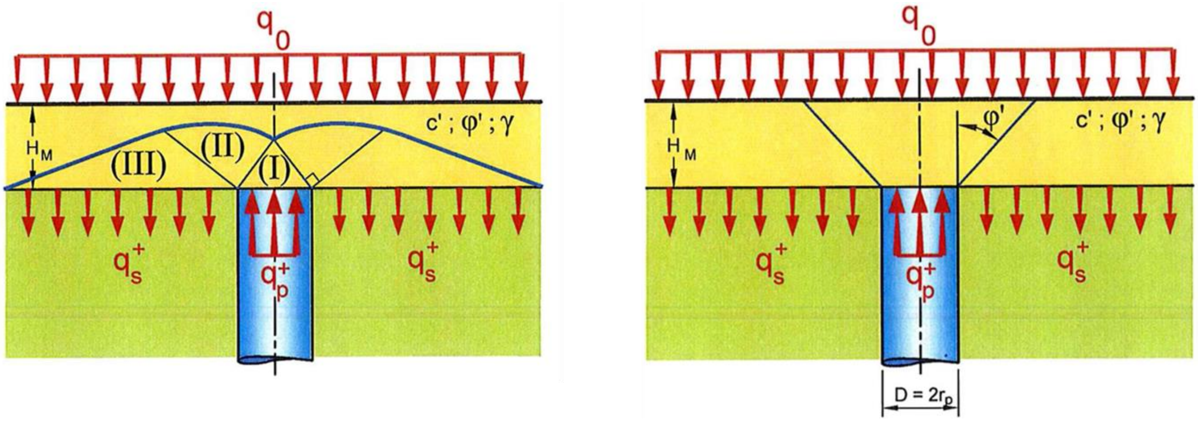

(a) (b)

Fig. 8. (a) Prandtl failure mechanism for slabs on grade, rafts or footings and thick embankments and (b) punching failure for thin embankments [8]

Prandtl's Failure Mechanism

As shown in Fig. 8(a), Prandtl's failure diagram includes a Rankine active limit state domain (I) above the inclusion head that is delimited by a logarithmic spiral arc domain (II) and a Rankine passive limit state domain (III) that is located beyond the inclusion head. In this figure q_p^+ is the stress at the inclusion head and q_s^+ is the stress on the in-situ soil.

ASIRI has been developed in line with Eurocode. The maximum load that can be applied to the inclusion head q_p^+ is therefore calculated in ULS (Ultimate Limit State) condition. This verification is performed by implementing Eurocode 7 [10] Design Approach 2 with the combination of partial factors being *A1* + *M1* + *R2* (*A* for Action, *M* for Material and *R* for Resistance), which means that load factors on dead and live loads are respectively 1.35 and 1.50 and that no partial factor is applied to the materials. According the Prandtl's diagram, q_p^+ can be determined from the stress applied on the supporting soil and the intrinsic parameters of the LTP:

$$q_p{}^+ = s_q N_q q_s{}^+ + s_c N_c \frac{c'}{\gamma_{c'}} - s_\gamma N_\gamma r_p \frac{\gamma}{\gamma_\gamma} \qquad 1$$

N_q, N_c and N_γ are coefficients that are a function of the friction angle of the LTP, and can be calculated from Eq. 2 to Eq. 4:

$$N_q = \tan^2\left(\frac{\pi}{4} + \frac{\varphi'/\gamma_{\varphi'}}{2}\right) \times e^{\pi \tan\left(\varphi'/\gamma_{\varphi'}\right)} \qquad 2$$

$$N_c = (N_q - 1)\cot\left(\varphi'/\gamma_{\varphi'}\right) \qquad 3$$

$$N_\gamma = 2(N_q - 1)\tan\left(\varphi'/\gamma_{\varphi'}\right) \qquad 4$$

$\gamma_{c'}$, $\gamma_{\varphi'}$, and γ_γ are the material partial factors and equal to 1.

The LTP's weight is typically neglected for a relatively thin platform, and the superficial (third) term in Eq. 1 is omitted.

For purely granular LTP, cohesion is zero, and the related term becomes null. Hence, Eq. 1 ~~is~~ becomes:

$$q_p{}^+ = s_q N_q q_s{}^+ \qquad 5$$

For axisymmetric or plane-strain conditions, s_q= 1, and a relationship is established in the form of Equation 6 between q_p and q_s that is only a function of φ'.

$$q_p{}^+ = N_q q_s{}^+ \qquad 6$$

Solving the problem and determining the values of q_p and q_s requires a second equation. Using load conservation:

$$\alpha q_p{}^+ + (1-\alpha) q_s{}^+ = q_o \qquad 7$$

α= replacement ratio [5, 6]

$$\alpha = \frac{A_c}{A_c + A_s} \qquad 8$$

A_c= area of inclusion

As= area of soil

From Equations 6 and 7 will yield:

$$q_p{}^+ = \frac{N_q}{1 + \alpha\left(N_q - 1\right)} q_o{}^+ \qquad 9$$

$$q_s{}^+ = \frac{1}{1 + \alpha\left(N_q - 1\right)} q_o{}^+ \qquad 10$$

Research on the Prandtl's failure mechanism has been further carried out by centrifugal testing with various LTP thicknesses, rigid inclusion spacing and replacement ratios within the ASIRI program. Centrifuge test results are compared with limiting pressures calculated from Prandtl's theory in Figure 5. Plotted points would fall on the bisecting line if there is a perfect agreement between measurements and theory. Using the friction angle at critical state, i.e. the red points in Figure 5), it can be observed that there is indeed a very close agreement.

The Prandtl approach was also investigated by performing finite element calculations for various uniformly distributed loads. In Fig. 10 the pressure acting on the soil and the pressure on the inclusion head are respectively shown on the abscissa and ordinate. The blue curve shows Eq. 6, the slanted black lines correspond to Eq. 7, and the pink line is derived from finite element calculations. This figure also presents the graphical solution of determining the stresses on the soil and inclusion head by intersecting Eq. 6 and Eq. 7, and the value that can be mobilized at the head of the inclusion.

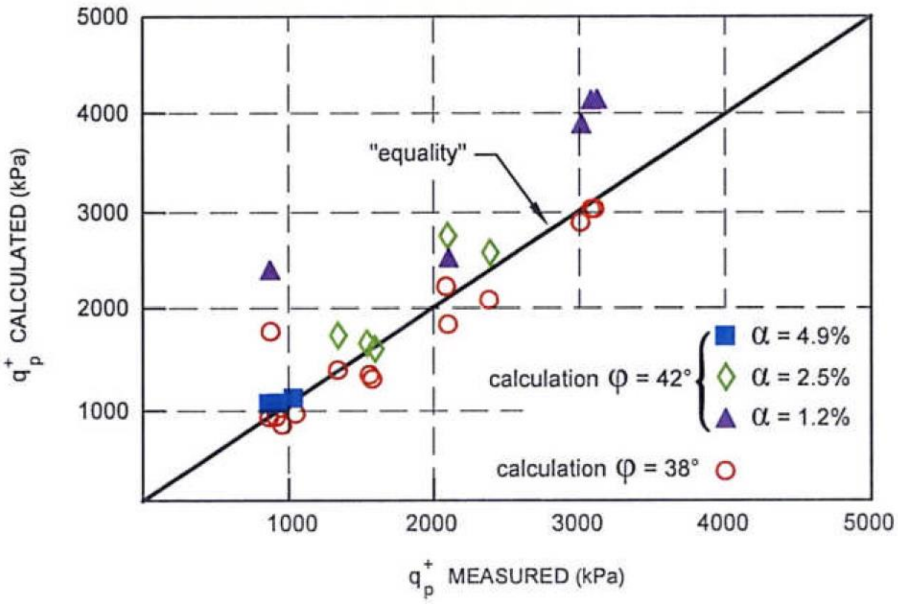

Fig. 9. Comparison of measured limiting pressures with theoretical values calculated from Prandtl's theory [8]

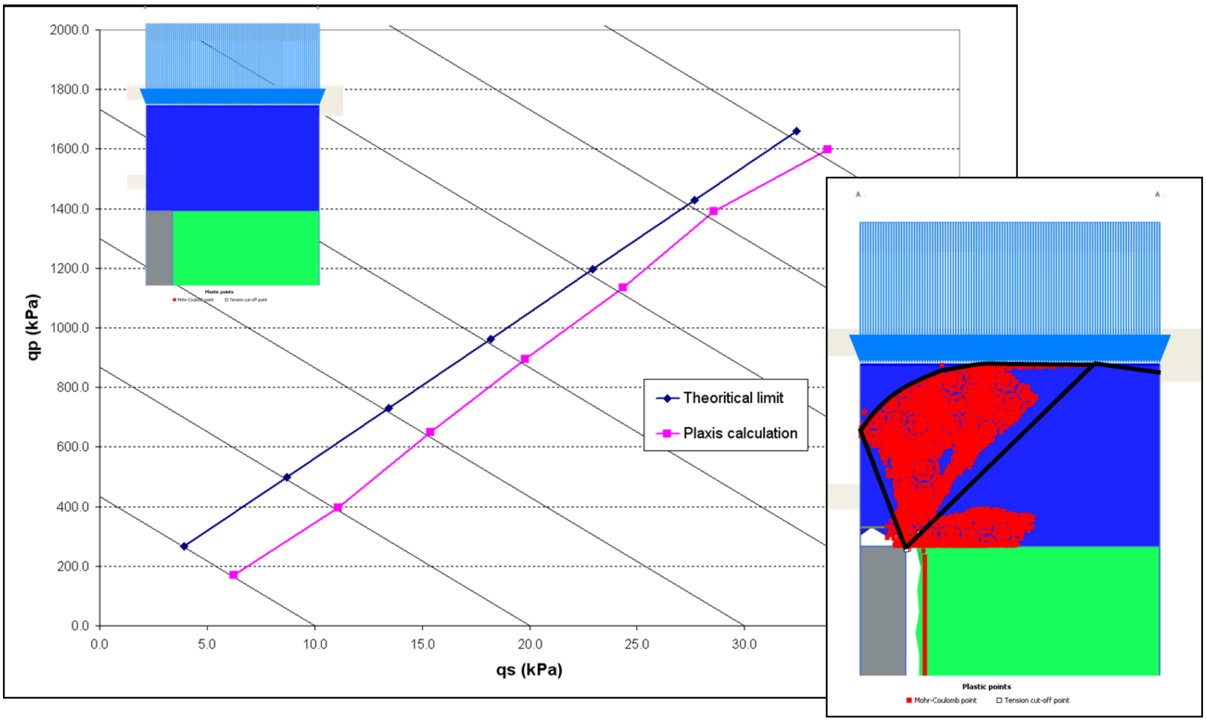

Fig. 10. Comparison of limiting pressures calculated from finite element analyses and Prandtl's theory [8]

During the investigation, using the same principle as moving the mobile bottom plate of centrifuge test, the Young modulus of the compressive soil was reduced for each uniform loading until the LTP failed. It was observed that at the last step prior to failure the stress at the inclusion head approached Prandtl limit but did not intersect it. Prandtl's failure mechanism can also be visualized by the distribution of the plastic points shown as red dots Fig. 10.

Punching Shear Failure Mechanism

As shown in Fig. 8(b) the second failure mechanism can be modeled by the realization of a vertical cone within the LTP layer. This mechanism exists only for thin LTP that are not covered by rigid structural elements, and is associated with the peak friction angle of the material.

According to Eurocode 7 Design Approach 2 and from the shear cone geometry, the limit stress at the inclusion head is determined using the applied external load, q_o, the LTP's thickness, and the platform parameters.

In Fig. 11 and Fig. 12:

$$R_c = R_p + H_M \tan\left(\frac{\varphi'}{\gamma_{\varphi'}}\right) \qquad 11$$

$$R = \frac{s}{\sqrt{\pi}} \qquad 12$$

As before $\gamma_{c'}$, $\gamma_{\varphi'}$, and γ_γ are the material partial factors and equal to 1.

If, as shown in Fig. 11, the shear cones do not overlap; i.e. if $H_M < H_c$, where:

$$H_c = \frac{R - r_p}{\tan\varphi'} \qquad 13$$

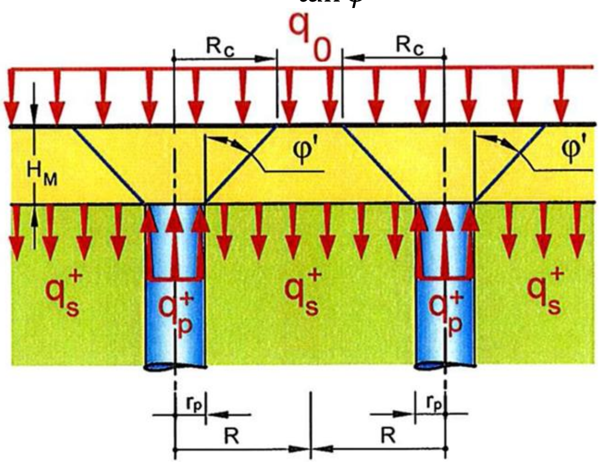

Fig. 11. Non-overlapping failure cones [8]

Then q_p^+= weight of the cone plus the external load applied on the top circular side of the cone. Thus:

$$q_p{}^+ = \frac{H_M}{3}\left(\frac{R_c{}^2}{r_p{}^2} + 1 + \frac{R_c}{r_p}\right)\frac{\gamma}{\gamma_\gamma} + \frac{R_c{}^2}{r_p{}^2}q + \frac{1}{\tan\varphi'}\left(\frac{R_c{}^2}{r_p{}^2} - 1\right)\frac{c'}{\gamma_{c'}} \qquad 14$$

If, as shown in Fig. 12, the shear cones overlap; i.e.

If $H_M > H_c$, where:

$$H_c = \frac{R_c - r}{\tan\varphi'} \qquad 15$$

and R_c= R, then q_p^+= weight of the cone, weight of the soil cylinder above it and the external load multiplied by the unit cell area. As before, partial factors from Eurocode 7 are included in these relations.

$$q_p{}^{+} = \left[\frac{H_M}{3}\left(\frac{R^2}{r_p{}^2} + 1 + \frac{R}{r_p}\right) + (H_M - H_c)\frac{R^2}{r_p{}^2}\right]\frac{\gamma}{\gamma_\gamma} + \frac{R^2}{r_p{}^2}q_o + \left[\frac{1}{\tan\varphi'}\left(\frac{R^2}{r_p{}^2} - 1\right)\right]\frac{c'}{\gamma_{c'}} \tag{16}$$

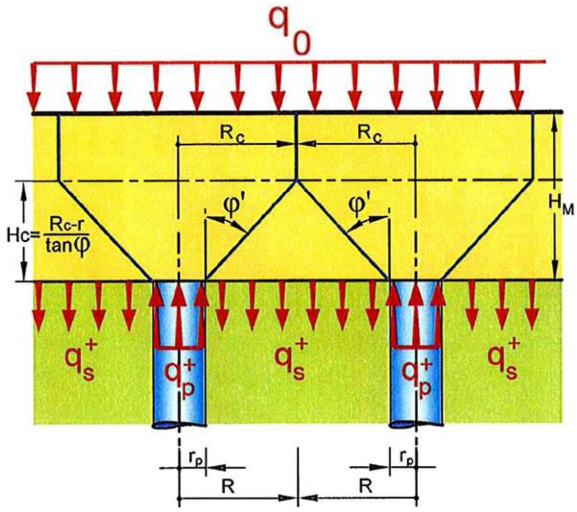

Fig. 12. Overlapping failure cones [8]

ULS Stress Domain

When failure is by Prandtl's mechanism, regardless of the load level, the stress domain in the LTP is firstly limited by the Prandtl line, which was presented in Eq. 6. The stress on the in-situ soil, $q_s{}^{+}$, is limited at ULS by the allowable stress $\sigma_{v;d}$, which can be determined with the appropriate partial factors from P_{LM}, the limit pressure of Menard pressuremeter test. Also, $q_p{}^{+}$ is limited by the load-bearing capacity of the inclusion as well as by the allowable stress in the inclusion material. The first limitation is the load bearing capacity as per Eurocode 7 and the second limitation, f_{cd}, is the allowable stress in the material as per Eurocode 2 [12]. The stress domain is graphically presented in Fig. 13.

$$q_{p\max} = \min\left[\frac{{}^{R_b}\!/_{\gamma_b \cdot \gamma_{R,d}} + {}^{R_s}\!/_{\gamma_s \cdot \gamma_{R,d}}}{\pi R_c{}^2}; f_{cd}\right] = \min\left[\frac{{}^{R_b}\!/_{1.375} + {}^{R_s}\!/_{1.375}}{\pi R_c{}^2}; f_{cd}\right] \tag{17}$$

$$\sigma_{v;d} = \frac{k_p P_{LM}}{\gamma_{R;v} \cdot \gamma_{R,d}} = \frac{k_p P_{LM}}{1.4 \times 1.2} = \frac{k_p P_{LM}}{1.68} \tag{18}$$

When the LTP is not covered by a rigid structural element, this domain may be partially limited. For example, as shown in Fig. 14, in the case of a thin LTP without rigid structural elements in which the failure cones do not overlap, the stress domain is further limited by the dashed blue line that corresponds to Eq. 14. As a second example that is shown in 15, further limitations that are shown as dashed red lines (Eq. 16) are applied when the failure cones overlap.

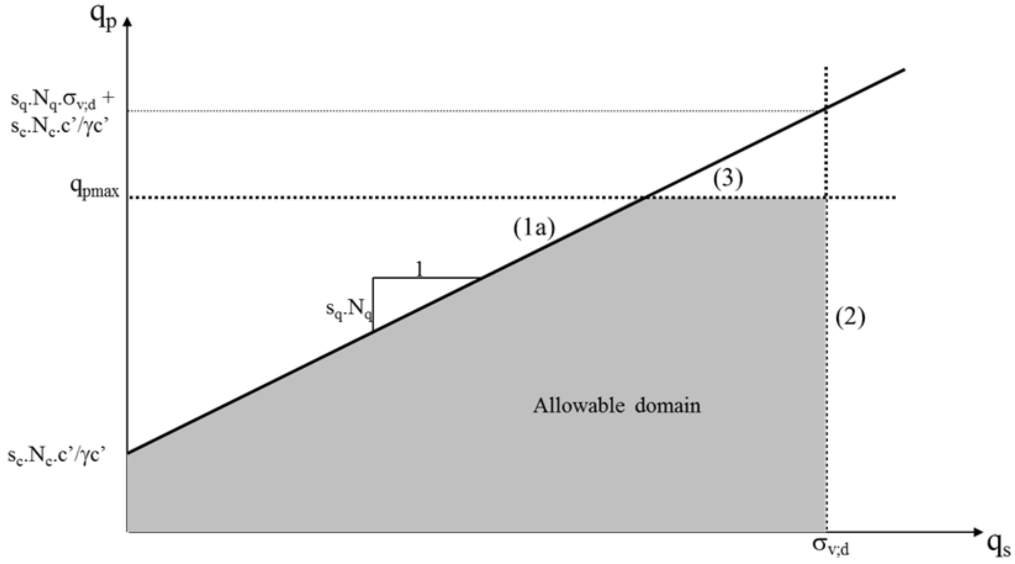

Fig. 13. ULS stress domain [8]

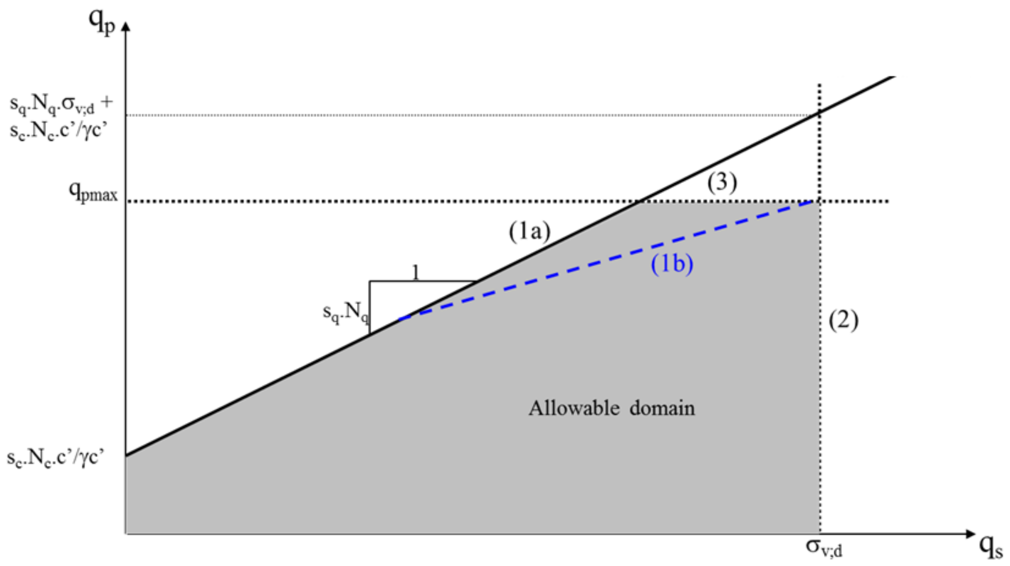

Fig. 14. ULS stress domain when LTP is thin, without rigid structural elements and with non-overlapping failure cones [8]

To satisfy the load conservation equation, $q_s{}^+$ and $q_p{}^+$ must be on the slanted blue line lines of Fig. 16. Therefore, for a given load q, the permissible domain is reduced to these segments. The calculated design limit $q_{p,d}{}^+$ is deduced by solving the system of 2 equations (Prandtl and load conservation). It is noted that if q increases $q_{p,d}{}^+$ will also increase.

$q_{p,d}{}^+$ depends on q, the system geometry (rigid inclusions grid size and thickness of LTP) and the LTP parameters, but is independent from the deformability of the various soil layers. While the intersection of Prandl's line (Eq. 14) and the load conservation line (Eq. 7) is $q_{p,d}{}^+$ the stress couple ($q_p{}^+$; $q_s{}^+$) that is actually mobilized can be anywhere on this slanted segment, and its actual position depends on the compressibility of the various soil layers directly below the LTP. If the soil is very soft, the mobilized couple will be close to $q_{p,d}^{+}$ and if the soil is quite dense, the couple will be away far from the limit.

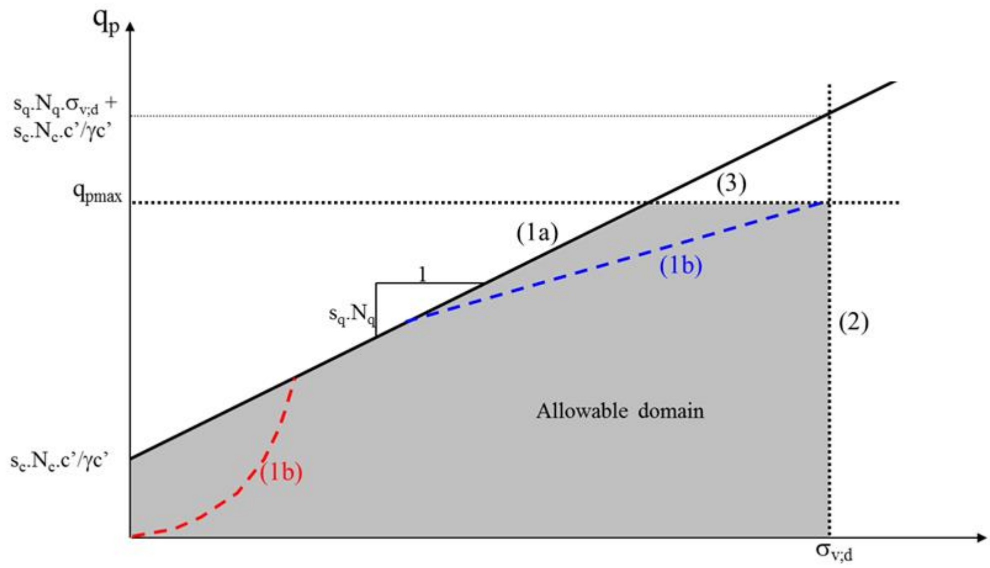

Fig. 15. ULS stress domain when LTP is thin, without a rigid structural element, and failure cones overlap [8]

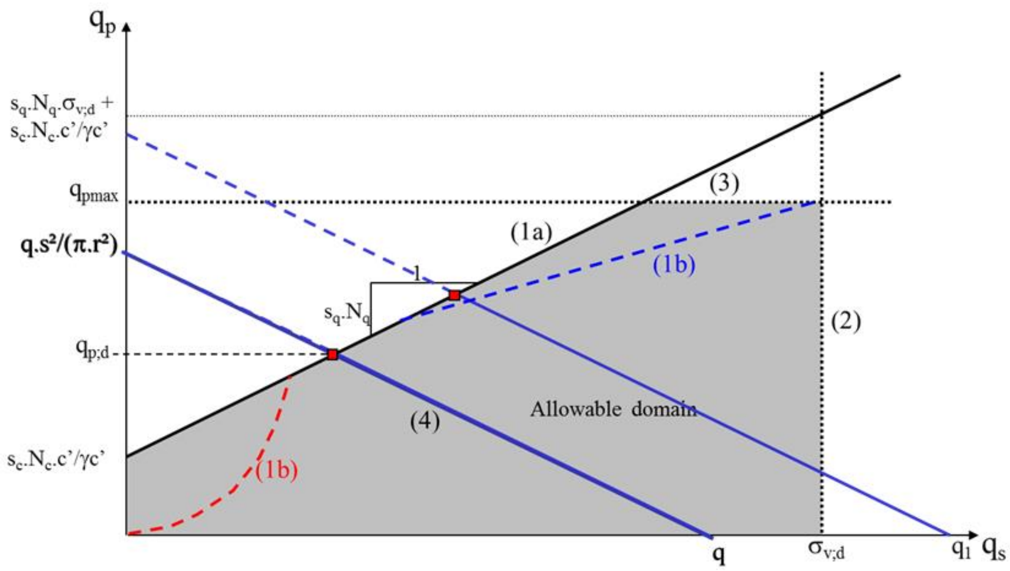

Fig. 16. ULS stress domain with consideration of the load conservation equation when LTP is thin, without a rigid structural element, and failure cones overlap [8]

It is important to note that, as shown in Fig. 17, changes of the external load moves the equilibrium in the plane (q_p^{+}; q_s^{+}) along a curve that for high loads tends towards an asymptote; i.e. the increase in loading increases the efficiency towards its maximum value, but is never able to create internal failure of the LTP by intersecting with Prandtl's line.

Edge Behavior

The focus of the previous sections of this paper was on the general behavior of the reinforced ground within the loading zone, away from the loading boundaries and where the

Prandtl failure mechanism fully developed. As shown in Fig. 18. The horizontal length of the Prandtl curve, L, is:

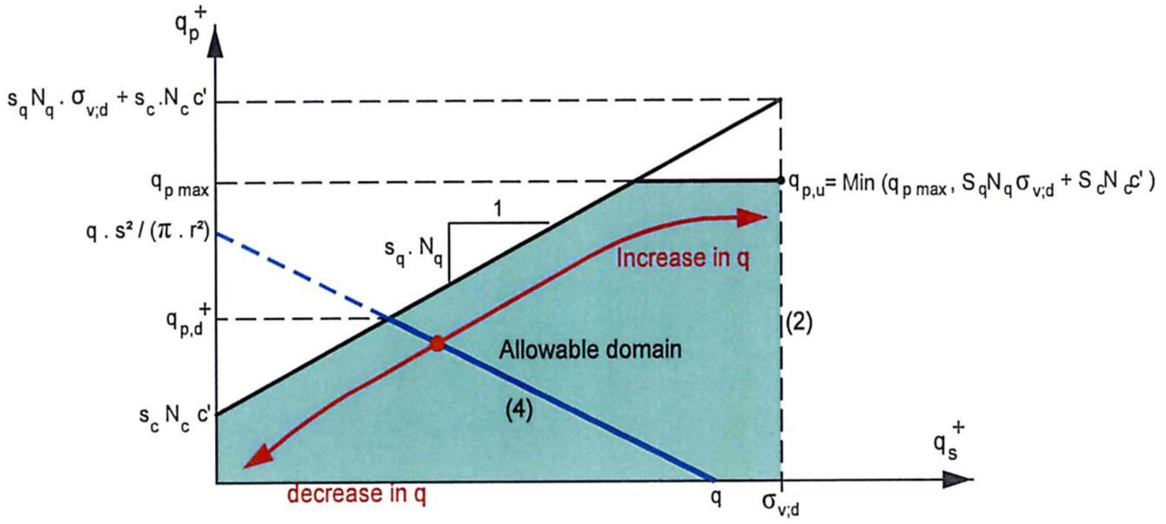

Fig. 17. $q_{p,d}^+$ and deformability of various soil layers [8]

$$L = \frac{\cos\left(\pi/_4 - \varphi'/_2\right)}{\cos\left(\pi/_4 + \varphi'/_2\right)} D e^{-\tan(\varphi').\pi/_2} \qquad 17$$

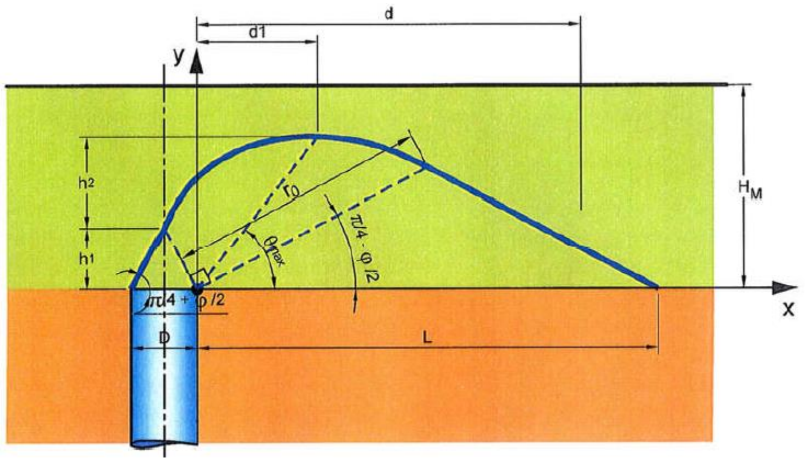

Fig. 18. Fully developed Prandtl spiral [8]

However, the distribution of stresses at the edge of the loading zone is different. As shown in Fig. 19(a), for cases in which the overhang of the footing is greater than when L has fully developed to L_{max}, and Prandtl's mechanism can fully develop in the LTP, the limit pressure at the inclusion head is as discussed. In the extreme case, shown in Fig. 19(b), the edge of the inclusion corresponds to the edge of the footing; i.e. overhang is zero, and the load applied to the footing is nearly fully transmitted on the inclusion head. The vertical stress on the peripheral soil is equal to γH, which is generated from the surrounding ground. ASIRI details the calculation process of N_q* with consideration of a LTP that is limited to the footing footprint. N_q* is assessed based on the friction angle at critical state of both the LTP (with φ_1) and the surrounding soil (with φ_2). N_q* values based on LTP and surrounding soil friction angles are shown in Table 1.

As graphically shown in Fig. 20, when the footing overhang is between 0 and L_{max} (refer to Fig. 19 (c)), the limiting pressure at the inclusion head can be estimated using a linear interpolation between these two extreme values.

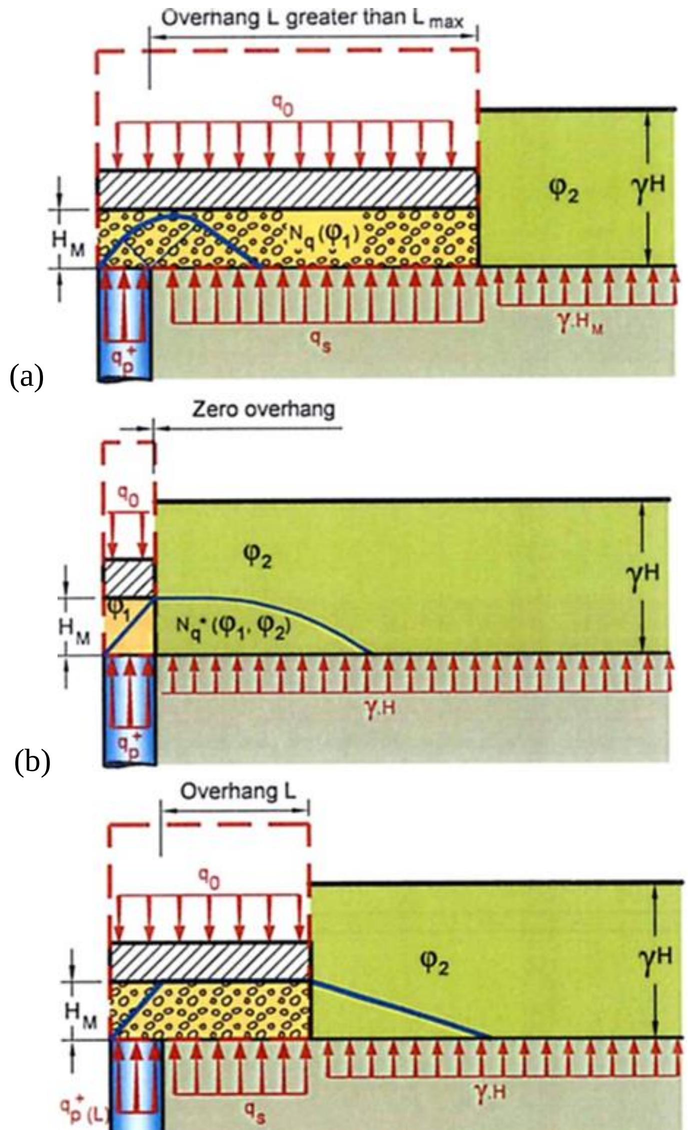

Fig. 19. Ground section at edge of rigid structural element [8]

In the general case when more than one inclusion is installed beneath the footing, the edge effect that has been described is applicable to only a fraction of the inclusion depending on whether the inclusion is located at a corner or side of the footing (see Fig. 21). The edge limit stress, $q_p{}^+(L)$, is applicable only to the exterior portion of the perimeter whereas the limit stress calculated from Prandtl’s failure mechanism, $q_p{}^+(P)$, applies to the interior portion of the inclusion. Hence, the resulting value must be a weighted average of these two terms.

By analogy with the distribution of negative friction within a group of piles, ASIRI proposes the following weighting relationships to determine the limit stress values on the inclusion head at different locations of the inclusions under the footing.

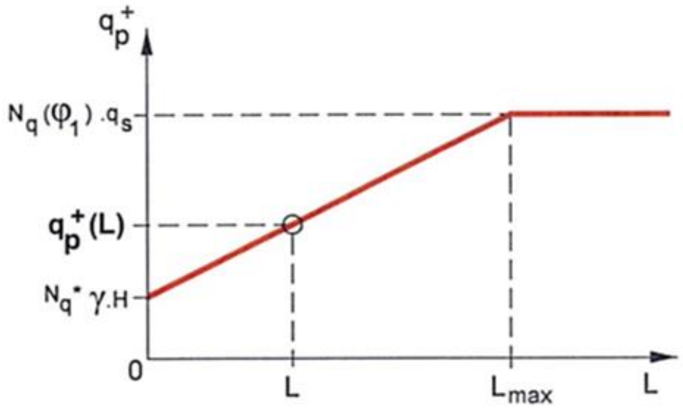

Fig. 20. Ground section at edge of rigid structural element [8]

Table 1

N_q* values based on LTP and surrounding soil friction angles

LTP φ_1	$N_q*(\varphi_1)$	Soil φ_2= 15°	Soil φ_2= 20°	Soil φ_2= 25°	Soil φ_2= 30°
		N_q*	N_q*	N_q*	N_q*
30	18.4	6.98	9.45	13.08	18.43
33	26.1	7.86	10.64	14.71	20.88
35	33.3	8.52	11.53	16.01	22.67
38	48.9	9.68	13.05	18.11	25.80
40	64.2	10.54	14.29	19.71	28.04

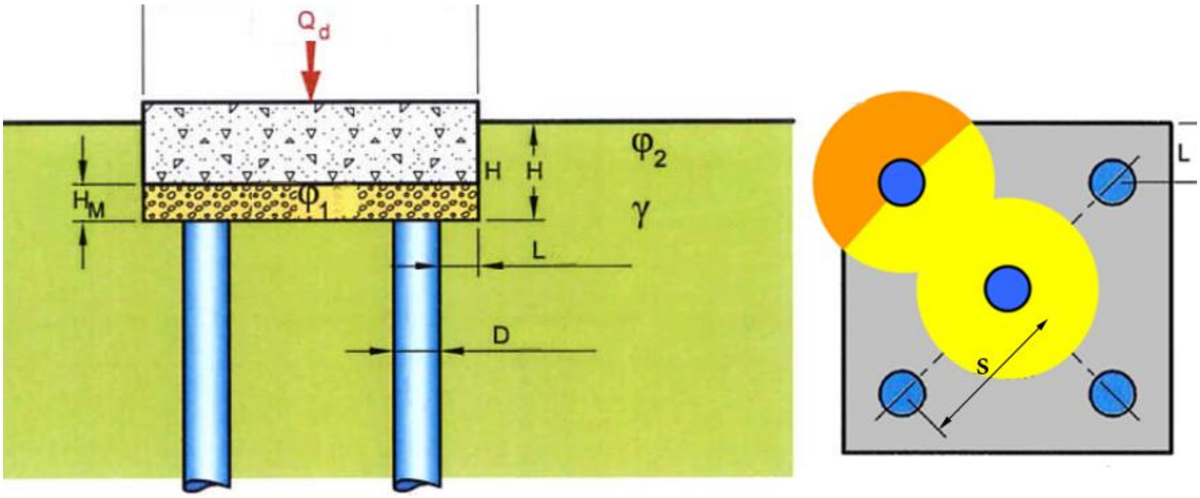

Fig. 21. Edge effect combination, modified from ASIRI [8]

Single row inclusion (see Fig. 22):

$$q_{p,a}{}^+ = \frac{1}{3} q_p{}^+(P) + \frac{2}{3} q_p{}^+(L) \quad 18$$

$$q_{p,e}{}^+ = \frac{2}{3} q_p{}^+(P) + \frac{1}{3} q_p{}^+(L) \quad 19$$

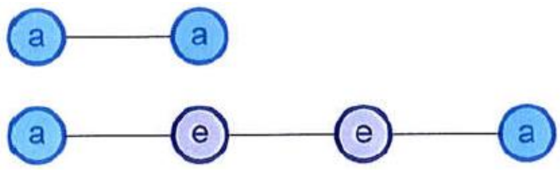

Fig. 22. Edge effect combination for single row of inclusions [8]

Multiple rows of inclusion (see Fig. 23):

$$q_{p,i}{}^{+} = q_p{}^{+}(P) \tag{20}$$

$$q_{p,a}{}^{+} = \frac{7}{12} q_p{}^{+}(P) + \frac{5}{12} q_p{}^{+}(L) \tag{21}$$

$$q_{p,e}{}^{+} = \frac{5}{6} q_p{}^{+}(P) + \frac{1}{6} q_p{}^{+}(L) \tag{22}$$

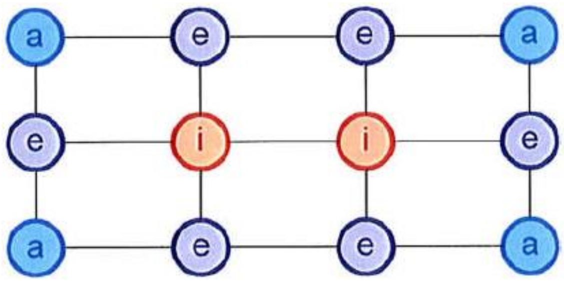

Fig. 23. Edge effect combination for multiple rows of inclusions [8]

It is to be noted that, as applicable to any geotechnical calculation, the accuracy of calculations is dependent on the value of the involved parameters, and inaccurate, scattered or unrepresentative values that may be chosen for cohesion, friction angle, unit weight, etc. will impact the results. Field tests that are carried out on site for verification of the results do not measure any of the parameters that have been described and the required values can only be estimated by correlation; therefore it may be beneficial to develop design procedures that are based directly on measured parameters such as the pressuremeter limit pressure and deformation modulus.

Case Study: Oil Tanks on the Banks of the Mississippi River

As part of the development program of an oil terminal located on the banks of the Mississippi River in New Orleans five steel tanks, each 12.8 m high are being constructed [13] Three tanks have diameters of 39.6 m and the other two tanks' diameters are 45.7 m. The tanks will exert a maximum pressure of 130 kPa to the ground, and elevating the ground level to tank level will impose an additional 16 kPa of pressure.

Below a superficial fill layer of approximately 0.15 to 1.2 m soft to medium stiff silty clays with some trace of organic matter and localized sand pockets extend down to a depth of 4 to 6 m. This layer is followed by very soft clay with silt and sand which reach depths of 20 to 24 m. A thin sand layer has also been identified at an approximate depth of 21 m. Medium stiff to stiff clay with fine sand pockets and shell fragments are observed to depths of up to 32 m followed by stiff to very stiff silty to sandy clays over a very dense layer of silty sands at depth of about 34 m. Groundwater level is quite high and at less than 1 m below ground level.

Project specification stipulated that the tanks' maximum and central settlements be limited to respectively 200 and 100 mm and additionally 50% of settlements allowed by American Petroleum Institute [14] three years after hydrotesting. However these criteria could not be satisfied due to the poor ground conditions and consequently a ground improvement contract was awarded to a specialist geotechnical contractor.

As the soil investigation indicated a reduction in compressibility at the depth of about 21 m at the level of the thin sand layer it was decided to install CMC with a higher replacement ratio down to the depth of the sand layer and a with a reduced replacement ratio down to the maximum treatment depth at about 34 m.

Due to the variations in the soil profile it was necessary to design each tank individually. Analyses included three dimensional digital modeling of a quarter of a tank, three dimensional modeling of a thin slice of the tank and manual calculations of rafts on floating piles.

CMC diameters for columns installed to approximately 21 m and 34 m were respectively 318 and 470 mm (see Fig. 24 for installation). Installation depth was variable for each tank due to variations in the site's soil profile.

Fig. 24.   Installation of 34 m long CMC

To confirm design, a large scale zone load test was carried out on site on an area of 13.7 by 13.7 m^2 loaded to the maximum design load. Vibrating wire piezometers, vibrating wire rebar strain gages, multi depth settlement gages, horizontal extensometer, inclinometers and settlement plates were used to measure ground behavior for a period of slightly less than three months. Maximum settlement measured at the top of the load transfer platform was 107 mm for a settlement plate located in between two columns, and minimum settlement was 64 mm for a settlement plate placed directly on top of a column at the bottom of the load transfer platform level. Maximum differential settlement was measured to be 43 mm between a CMC and the grid centre.

Further numerical modeling was carried out to compare actual measurements with calculated figures. Numerical analysis suggested a maximum settlement of 97 mm during the trial period which was in good agreement with actual measurements.

Conclusion

CMC is a modern ground improvement technology with numerous advantages, which include independence of column strength from in-situ soil parameters, independence of column lateral stability from in-situ soil parameters, ability to reduce settlements more than competing alternative columnar inclusion techniques with the same replacement ratio, vibration-less penetration auger that also produces negligible amounts of spoil per inclusion, and high production rates.

This technology utilizes a load transfer platform to distribute the loads between the columns and the in-situ ground. Column loads can be determined by numerous methods. More recently, the French developed a national research program called ASIRI to analyze ground behavior and load distribution for grounds improved with columnar inclusions in a variety of cases. ASIRI methods are based on Mohr-Columb parameters that are not directly measured by field tests, and it is proposed that further research be carried out to formulate calculation methods based on field measured parameters such as the pressuremeter limit pressure and deformation modulus.

References

1. Chu, J., Varaksin, S., Klotz, U. & Mengé, P. (2009) State of the Art Report: Construction Processes. *17th International Conference on Soil Mechanics & Geotechnical Engineering: TC17 meeting ground improvement,* Alexandria, Egypt, 7 October 2009, 130.
2. Hamidi, B., Nikraz, H. & Varaksin, S. (2009) Arching in Ground Improvement. *Australian Geomechanics Journal,* 44, 4 (December), 99-108.
3. Barksdale, R. D. & Bachus, R. C. (1983) Design and Construction of Stone Columns, Volume 1, FHWA/RD-83/026. 194.
4. Masse, F., Pearlman, S. L. & Taube, M. G. (2009) Controlled Modulus Columns for Support of above Ground Storage Tanks. *40th Ohio River Valley Soil Seminar (ORVSS),* Lexington, Kentucky, November 13.
5. Murayama, S. (1962) Vibro-Compozer Method for Clayey Ground (in Japanese). *Mechanization of Construction Work,* 150, 10-15.
6. Aboshi, H., Ichimoto, E. & Harada, K. (1979) The Compozer: A Method to Improve Characteristics of Soft Clays by Inclusion of Large Diameter Sand Columns. *International Conference on Soil Reinforcement; Reinforced Earth and Other Techniques,* 2, Paris, 20-22 March, 211–216.
7. Combarieu, O. (1988) Amélioration des sols par inclusions rigides verticales. application à l'édification de remblais sur sols médiocres. *Revue Française de Géotechnique,* 44, 57-79.
8. IREX (2012) Recommandations pour la conception, le dimensionnement, l’exécution et le contrôle de l’amélioration des sols de fondation par inclusions rigides, ASIRI 384, Presses des Ponts
9. Prandtl, L. (1920) *Uber Die Härte Plastischer Körper, Nachrichten von Der Königlichen Gesellschaft Der Wissenschaften, Gottingen, Math.- Phys. Klasse,*74-85.
10. European Standard (2004) EN 1997-1: 2004, Eurocode 7: Geotechnical Design - Part 1: General Rules 171.
11. Okyay, U. S. (2010) Etude expérimentale et numérique des transferts de charge dans un massif renforcé par inclusions rigides. application à des cas de chargements

statiques et dynamiques. *Civil and Environmental Engineering.* Lyon, Institut National des Sciences Appliquées de Lyon, 402.

12. European Standard (2004) BS EN 1992-1-1, Eurocode 2: Design of Concrete Structures – Part 1-1: General – Common Rules for Building and Civil Engineering Structures.
13. Buschmeier, B., Masse, F., Swift, S. & Walker, M. (2012) Full Scale Instrumented Load Test for Support of Oil Tanks on Deep Soft Clay Deposits in Louisiana Using Controlled Modulus Columns. *International Symposium on Ground Improvement (IS-GI) Brussels 2012*, 3, Brussels, 31 May - 1 June, 359-372.
14. American Petroleum Institute (2001) API Standard 653: Tank Inspection, Repair, Alteration, and Reconstruction, 3rd Edition, 112.